

Across-wind excitation mechanism for interference of twin tall buildings in tandem arrangement

G.B. Zu^{1a} and K.M. Lam^{*2}

¹Department of Civil Engineering, The University of Hong Kong, Pokfulam, Hong Kong

²Department of Civil and Environmental Engineering, The Hong Kong University of Science and Technology, Clear Water Bay, Hong Kong

(Received June 15, 2017, Revised January 24, 2018, Accepted March 21, 2018)

Abstract. Excitation mechanism of interference effect between two tall buildings is investigated with wind tunnel experiments. Synchronized building surface pressure and flow field measurements by particle image velocimetry (PIV) are conducted to explore the relationship between the disturbed wind flow field and the consequent wind load modification for twin buildings in tandem. This reveals evident excitation mechanisms for the fluctuating across-wind loads on the buildings. For small distance ($X/D < 3$) between two buildings, the disturbed flow pattern of impaired vortex shedding is observed and the fluctuating across-wind load on the downstream building decreases. For larger distance ($X/D \geq 3$), strong correlation between the across-wind load of the downstream building and the oscillation of the wake of the upstream building is found. By further analysis with conditional sampling and phase-averaged techniques, the coherent flow structures in the building gap are clearly observed and the wake oscillation of the upstream building is confirmed to be the reason of the magnified across-wind force on the downstream building. For efficient PIV measurement, the experiments use a square-section high-rise building model with geometry scale smaller than the usual value. Interference factors for all three components of wind loads on the building models being surrounded by another identical building with various configurations are measured and compared with those from previous studies made at large geometry scale. The results support that for interference effect between buildings with sharp corners, the length scale effect plays a minor role provided that the minimum Reynolds number requirement is met.

Keywords: high-rise buildings; wind loads; interference effect; Reynolds number; PIV

1. Introduction

Interference effect on overall wind loads and wind-induced responses of two or more buildings in proximity has been extensively studied, mostly with wind tunnel experiments (e.g., Bailey and Kwok 1985, Khanduri *et al.* 2000, Lam *et al.* 2008, Taniike 1992, Xie and Gu, 2007, Yu *et al.* 2016). In recent years, some attention is focused on local wind pressure modification for its importance in cladding design (Hui *et al.* 2012, Kim *et al.* 2011, Yu *et al.* 2015). All those studies provide not just large amounts of useful data to enrich the database of building interference but also suggest empirical formulas for evaluating local and overall wind loads for certain building geometries and arrangement patterns.

Modification of wind loads induced by interference effect from surrounding buildings depends on many parameters, such as geometry and arrangement of buildings, terrain type and turbulence intensity of approaching flow. The possible combinations of these parameters are too large to be covered exhaustively. Therefore, a more physically-based approach, such as investigating the underlying mechanisms of interference effect, would be worth adopting

to solve the problem. Some efforts, such as the following examples have been made to understand various interference mechanisms.

Bailey and Kwok (1985) measured the velocity spectrum in the wake of a tall building model with and without an identical upstream building in tandem arrangement and found that the periodic vortex shedding was quite obvious for the isolated building but totally disappeared for the building with an upstream building. They concluded that the upstream building had a disruptive effect on the vortex shedding of the downstream building. Under this situation, the across-wind fluctuating energy on the downstream building mainly came from the approaching flow. This finding was confirmed by flow visualization experiments conducted by Taniike (1992) which also found that fluctuating drag on a downstream building increased as the size of the upstream building increased because the larger building width increases the scale of the shed vortices. Sakamoto and Haniu (1988) observed the reattachment of shear layer of an upstream building onto the side surface of the downstream building in several different staggered arrangements by smoke visualization technique. Gowda and Sitheeq (1993) visualized the flow pattern between two tandem twin buildings and found that the downstream building experienced three stages, namely, submergence in the shear layers, being attacked by the shear layer directly on the windward surface and insusceptibility to the interference, as the spacing between two buildings changed from small to

*Corresponding author, Associate Professor

E-mail: kitminglam@ust.hk

^a Ph.D Candidate

large values. Hui *et al.* (2013b) observed the flow pattern between two rectangular-section high-rise buildings and found that peak pressure on the downstream building were usually caused by the shear layer from the upstream building. Findings in many of the above-described studies are made from flow visualizations in which wind flow pattern between two tall buildings and its possible connection with resulted wind load were qualitatively observed and analyzed. Despite these studies, the exact interference mechanisms between two high-rise buildings still remain not clear. The lack of a detailed investigation of the instantaneous wind flow patterns around the two buildings under interference is perhaps the missing link for the understanding of the interference mechanism. This is exactly the objective of this paper to report and document detailed wind flow patterns responsible for the interference effects between two tall buildings.

Recently, due to the rapid development of flow analysis software and hardware, detailed spatial and temporal information of the flow field can be studied quantitatively by techniques such as particle image velocimetry (PIV). Hui *et al.* (2013a) observed instantaneous and time-averaged flow field between two buildings with rectangular and square sections with PIV. Kim *et al.* (2013) performed simultaneous pressure and flow field measurements on two identical square-shape building models in the side-by-side and staggered arrangements. PIV measurement of flow field can provide quantitative flow results such as mean and fluctuating wind speed, thus making it a useful tool to study the mechanism of interference effect, especially when combined with simultaneous measurement of wind loads on the buildings (e.g., Cheng and Lam 2015)

This paper focuses on the underlying interference mechanism of twin tall buildings in tandem arrangement. The main objective is to investigate the instantaneous wind velocity fields past the two buildings with PIV and to unveil the flow excitation mechanisms for the interference effects on dynamic wind loads on the buildings. In the tandem arrangement, the along-wind force on the downstream building always experiences shielding provided by the upstream building, but the fluctuating across-wind force can be largely magnified for certain distances between the buildings. It is believed that the periodic vortex shedding from the downstream building is disrupted and the narrow-banded across-wind force on the downstream building is attributed by the upstream building wake. However, the exact coherent structure of flow around the buildings and its role in force excitation on the downstream building remain unclear without detailed measurement of the wind flow fields. It is the key objective of this paper to explore the exact excitation mechanism for the modification of across-wind forces on the two buildings arranged in tandem.

Concurrent with measurements of flow field past the two buildings by PIV, wind pressures on the building surfaces are measured in synchronization with PIV. The characteristics of the wind flow field and the consequent wind pressure distribution are studied by analyzing both instantaneous and time-averaged results. The flow field and pressure data are further analyzed with the conditional sampling technique to study the relationship between wind

flow pattern and fluctuating wind pressures on the downstream building during the occurrence of peak wind force events. The phase averaging technique, based on Hilbert transform, is further employed to detect coherent structures from the turbulent wind load signals and to determine the phase of the coherent structures corresponding to the consequent fluctuating across-wind force on the downstream building.

It is known that the influence of an upstream building on a downstream building can exist even for spacing between two buildings as large as 10 times of the building width. When PIV measurement is used in wind tunnel testing of building interference, the testing area could be too large to capture if building models with normal dimension are used. As a solution, PIV measurements in the present study are made on wind tunnel models at a geometry scale of 1:1000, which is smaller than the typical scale of 1:400 to 1:200 used in most previous wind tunnel investigations of building interference. Although the Reynolds number (Re) of the wind tunnel tests still satisfies the minimum requirement of $Re = 1.1 \times 10^4$, for sharp-edged structures (ASCE 2012), its value is notably smaller than the Re values around $2 \sim 4 \times 10^4$ used in most previous studies on interference effect. Some wind tunnel testing guidelines, such as AWES (2001), recommend a minimum Reynolds number at 5×10^4 and a minimum geometric scale of 1:800 for tall building models. Furthermore, flow over some bluff bodies with a large aspect ratio can be sensitive to Reynolds number change as they are easily affected by the separated shear layers, which are more sensitive to Reynolds number effect (Larose and D'Auteuil 2006). Therefore, the first part of this paper is devoted to a study of the effect of model scale and the validation of Reynolds number independence of the present wind tunnel tests.

2. Experimental setup

2.1 Pressure measurement test

Experiments were carried out in the boundary layer wind tunnel in the Department of Civil Engineering at the University of Hong Kong. The working section was 3.0 m wide, 1.8 m tall and 12 m long. Wind tunnel tests were carried out under simulated wind flow of the open land terrain, where the mean wind profile followed the power law with a power exponent of 0.11. The flow in the wind tunnel was interpreted at a geometrical scale targeted at 1:1000. The mean wind speed and turbulence intensity at the height of the building model during the test were $U_H = 8.7$ m/s and 0.089, respectively. The measured mean wind velocity and turbulence intensity profiles are shown in Fig. 1.

Two building models of identical sizes and shapes were used in the experiments. Measurements were made on a rigid pressure model, referred to as the principal building, while the other model was not installed with any instrument, referred to as the interfering building. Both building models had a square-plan form of breadth $D = 30$ mm. The height-to-breadth ratio was $H/D = 6$. At the target geometric scale

1:1000, the models represented full-scale buildings of height 180 m and width 30 m. The Reynolds number of the testing was $Re = U_H D / \nu \approx 1.8 \times 10^4$. A total of 120 pressure taps, 30 on each of its four surfaces, were installed on the walls of the principal building (Fig. 2). A multi-port pressure scanning system (Initium from PSI, Inc.) measured the wind pressures at all taps on a building model at a sampling rate of 333 Hz per port for a length of 60 s.

For the study of model scale effect and Reynolds number independence, interference effect was measured on a grid of different relative locations of the two buildings. Fig. 3 shows the different arrangement configurations of the buildings and the coordinate system which follows that used by Mara *et al.* (2014) to which the present interference effects are compared. With the principal building located at $(X/D = 0, Y/D = 0)$, the locations of the interfering building ranged from $X/D = 0$ to 10 and from $Y/D = 0$ to 5 with an interval of $0.5D$ except for a small area ($X/D = 0 \sim 1, Y/D = 0 \sim 1$) where the two buildings could not be physically placed. The combination of longitudinal and lateral building separations resulted in 222 configurations. The two building models were both orientated at normal wind incidence.

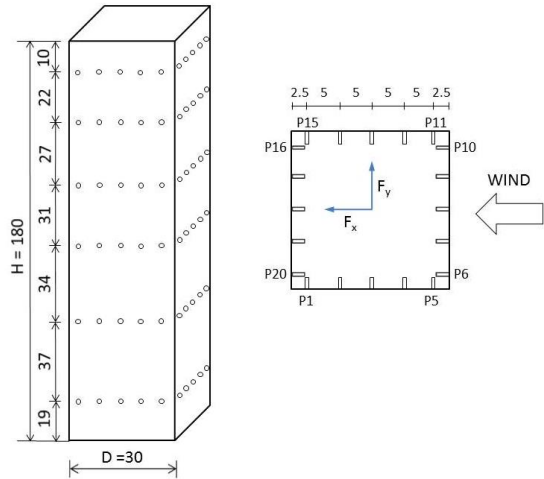
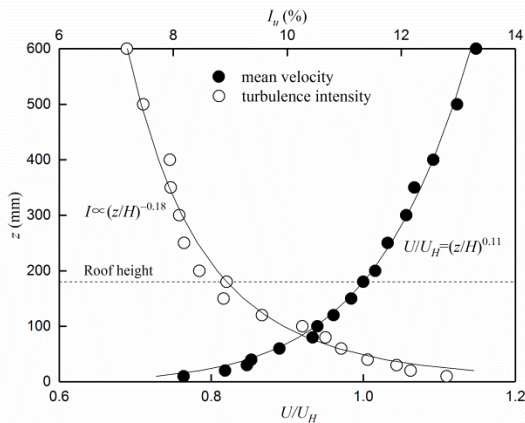
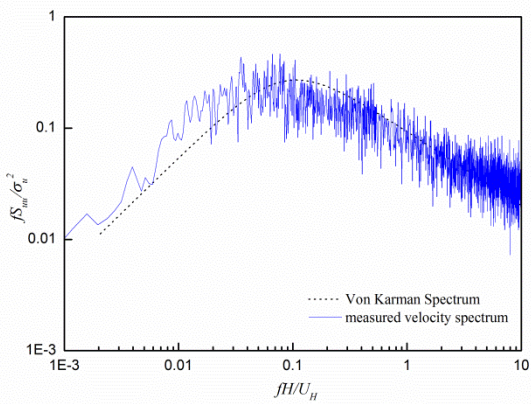


Fig. 2 Layout of pressure taps on principal building model (unit: mm)



(a) Mean wind speed and turbulence intensity profiles



(b) Longitudinal turbulence spectrum

Fig. 1 Wind characteristics in wind tunnel

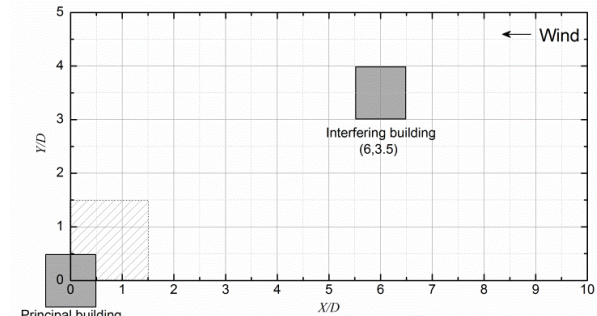
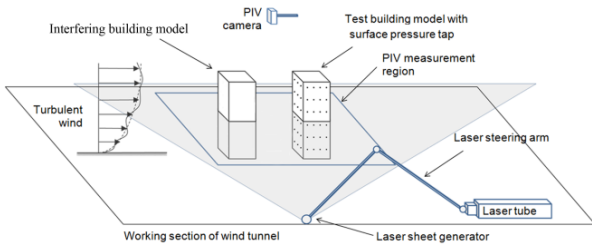


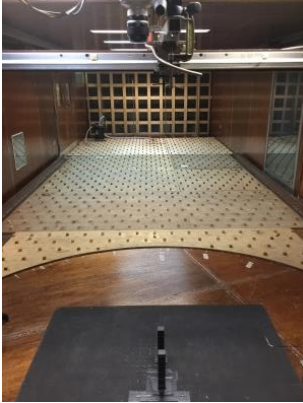
Fig. 3 Coordinate grid for location of interfering building

2.2 Synchronized pressure and flow field measurement

A time-resolved PIV system measured the instantaneous velocity fields on a horizontal plane through the two buildings. The measurement plane was illuminated by a thin laser sheet generated from the laser beam of a double-cavity Q-switched Nd:YAG laser (Nano 50-100, Litron). The laser sheet generator and the laser steering arm were placed inside the working section of the wind tunnel and downstream of the building model. A 1:1 mixture of DEHS liquid and sunflower seed oil was used to produce seeding particles using a high volume liquid seeding generator (10F03, Dantec Dynamics). The particles had diameters at about 2 to 5 μm and could satisfactorily scattered the laser light in the air flow when viewed as a small region of interest. Flow images were captured with a high-speed CMOS camera (SpeedSense, Dantec Dynamics). The camera had a high sensitivity for the weak scattered light signals in air flow with resolution at 1920×1200 pixels. The camera framing speed was set at 100 double-image/s to capture a time sequence of particle images of 1825-image length. A time interval 0.12 ms was used between the double laser pulses to fix the initial and final positions of seeding particles in the double image. The PIV analysis



(a) PIV arrangement for buildings



(b) Photo of wind tunnel test

Fig. 4 PIV set-up in wind tunnel

software was based on the adaptive PIV algorithm (Theunissen *et al.* 2010, Willert and Gharib 1991). In the final iteration, PIV vectors were obtained on interrogation areas of size 12×12 pixels. The number of velocity vectors were 160×100 and the physical resolution of each vector was about $2.4 \times 2.4 \text{ mm}^2$.

In order to synchronize the pressure measurement and flow field acquisition by PIV, pressure measurement was triggered by the framing signals of the PIV camera. This synchronization ensured that the pressure scanning was made at the same instants when the PIV camera captured the double-images of the flow and that both sampling was made at 100 Hz. Fig. 4 shows the PIV set-up in the wind tunnel.

3. Results and discussions

Section 3.1 investigates the effect of small geometric scale and Reynolds number on the wind tunnel experiments of building interference. Wind pressure measurements were carried out for the principal building without the interfering building and, then, with the interfering building placed at the planned locations. The results are compared with those of Mara *et al.* (2014) which were obtained at a larger geometric scale of 1:400 and a higher Reynolds number. In Section 3.2, the excitation mechanism of two interfering buildings in different tandem arrangements are studied with synchronized pressure and flow visualization measurements.

3.1 Interference factor (IF) and Reynolds number independence

From the measured pressure signals on the four walls of the principal building, aerodynamic forces acting on the model were calculated by means of pressure integration as

$$M_a = \sum_{i=1}^N p_i A_i n_{i,along} h_i \quad (1)$$

$$M_c = \sum_{i=1}^N p_i A_i n_{i,cross} h_i \quad (2)$$

$$T_z = \sum_{i=1}^N \pm p_i A_i d_i \quad (3)$$

where M_w , M_c and T_z are the along-wind moment, across-wind moment and torsion, respectively. p_i , A_i and h_i are the pressure, tributary area and height of tap (i), $n_{i,along}$ and $n_{i,cross}$ are unit direction cosines to the surface, and d_i is the distance of tap i to the central axis of the building.

The interference effects on the three overall moments on the principal building are summarized in the form of interference factor that depicts the change of aerodynamic force acting on the principal building due to interference from the neighboring building. The interference factor (IF) suggested by Saunders and Melbourne (1980), is defined as

$$\text{Interference factor (IF)} = \frac{\text{Wind load (interfering buildings present)}}{\text{Wind load (isolated building)}} \quad (4)$$

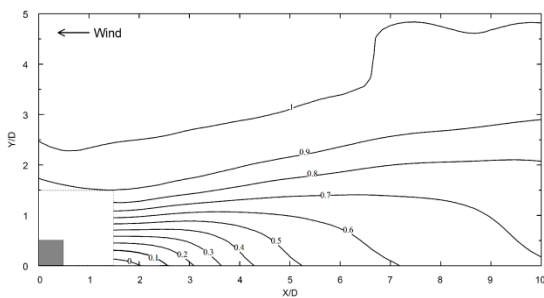
In many previous studies, the measured interference effects under different locations of the interfering building were summarized as contour plots of IF (Kim *et al.* 2013, Taniike and Inaoka 1988). Most early studies were carried out in uniform or low turbulent wind conditions (Khanduri *et al.* 2000, Sakamoto *et al.* 1987, Taniike 1992). However, Kareem (1987) has found that interference effect is sensitive to turbulence intensity of the approaching flow. Xie and Gu (2004) reported the IF contour of mean along-wind load for twin buildings under two terrain types. With experiments under the open land and urban terrain type, Mara *et al.* (2014) presented IF contour plots of along- and across-wind load and torsion with the interfering building on a dense grid from the principal building. That detailed study provides a good benchmark for comparison with the present results obtained at a smaller geometric scale. In the present study, interference factors of buildings with tandem, staggered and side-by-side arrangements are tested in the open land flow condition.

3.1.1 Along-wind IF

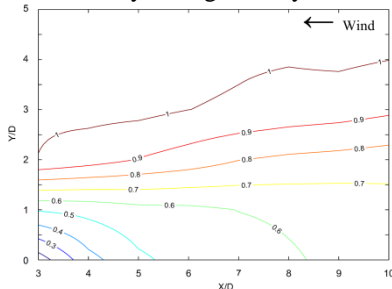
Contours of IF for the mean along-wind moments are shown in Fig. 5(a) for the present measurement at 1:1000. The result of Mara *et al.* (2014) is shown in Fig. 5(b) for comparison. That study tested two square-shaped building models with aspect ratio of 1:1.7 and at the geometric scale

of 1:400, giving Reynolds number of 2.4×10^4 . For the mean along-wind moment, it can be found that there is a great consistency between the two studies even for the small difference in aspect ratios. Similar to many previous studies (e.g., English 1993), the lowest IF is found in the tandem arrangement ($Y/D = 0$) where shielding effect plays a dominant role. The shielding effect decreases gradually as the distance between two buildings increases. The mean along-wind load becomes almost zero when the interfering building is positioned at ($X/D = 2, Y/D = 0$). The variations of IF of the time-averaged mean along-wind load on the downstream building with building separation in the tandem arrangement and side-by-side arrangement are presented in Fig. 6. The results are generally consistent with those of Sakamoto and Haniu (1988) and Taniike (1992), which were obtained at Reynolds number $Re = 5.1 \times 10^4$ and 2.9×10^4 , respectively. It is noted that the aspect ratios of tall building models in these two studies were 3 and 4.5, respectively.

Fig. 7 presents the IF contours for the root-mean-square (RMS) along-wind load. The results of present study and those of Mara *et al.* (2014) are very similar. Unlike the mean along-wind result that the interfering building always provides shielding for the principal building, an increase in RMS along-wind moment is found when two buildings are in the staggered arrangement. The greatest value of $IF = 1.27$ is observed at the location ($X/D = 3, Y/D = 1$) which is the exact same location reported by Khanduri *et al.* (2000) for the highest IF. In the tandem arrangement, the upstream building provides shielding for the downstream building with an IF between 0.7 and 0.9. The side-by-side arrangement can also lead to reduction of the RMS along-wind load when two buildings are closely positioned $Y/D < 3$ and the interference effect become negligible for locations $Y/D > 3$.

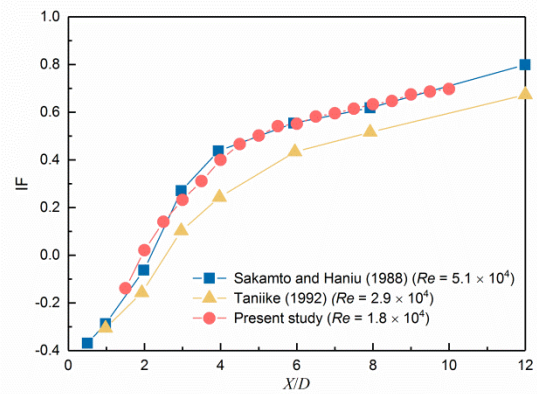


(a) Present study with geometry scale 1:1000

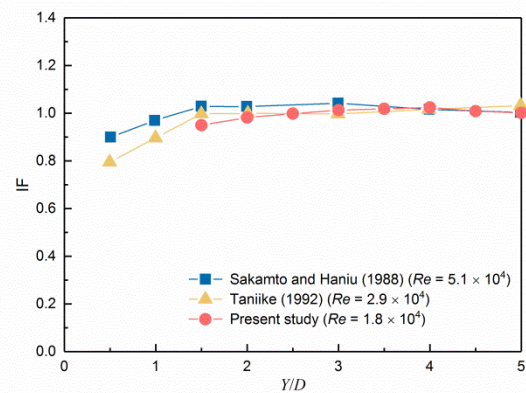


(b) Mara *et al.* (2014) with geometry scale 1:400

Fig. 5 IF contours of mean along-wind moment



(a) Tandem arrangement



(b) Side-by-side arrangement

Fig. 6 Comparison of mean along-wind force due to interference

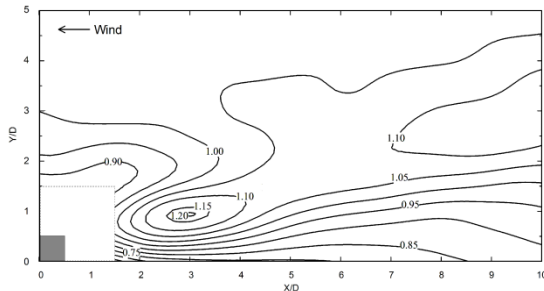
For buildings tested in low turbulence intensities, fluctuating along-wind load can be magnified by up to 50% when surrounded by a side-by-side interfering building (Taniike 1992). The lower turbulence in the approaching flow would result in a lower RMS along-wind load on the single isolated building, while the turbulence introduced by the surrounding building is more likely to play a dominant role in the modification of fluctuating along-wind load.

3.1.2 Across-wind IF

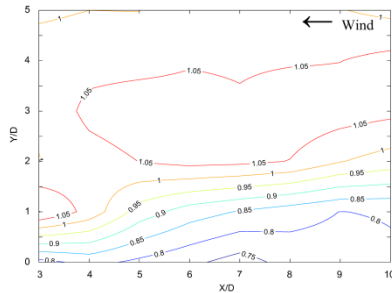
As the test buildings are symmetric and the flow direction is normal to the building surface, the mean across-wind load is zero in the single isolated building so that the IF becomes meaningless in Eq. (4). Contours of IF for the RMS across-wind IF are presented in Fig. 8. A well-defined region is observed in the staggered arrangement where IF is higher than unity. The peak location is found at ($X/D = 5, Y/D = 2.5$) where the greatest IF occurs at 1.61. This location of peak IF reported by Mara *et al.* (2014) is ($X/D = 5, Y/D = 3$) and the peak IF is between 1.4 and 1.5. It is noted that in their study the interval of the spacing variations is D instead of $D/2$ used in this study.

Table 1 Critical locations of interference on fluctuating across-wind load of two identical buildings with square cross-section, AR = aspect ratio, TI = turbulence intensity at building height

	Re	AR	TI	IF_{max}	(X, Y) of IF_{max}
Sakamoto and Haniu (1988)	5.1×10^4	3	not given	1.7~1.8	$(5D, 2.5D)$
Taniike (1992)	2.9×10^4	4.5	“low”	2.5~2.6	around $(6D, 3D)$
Khanduri <i>et al.</i> (2000)	not given	4	not given	1.6	$(4D, 2.5D)$
Mara <i>et al.</i> (2014)	2.4×10^4	7	10.2%	1.4~1.5	$(5D, 3D)$
Present study	1.8×10^4	6	8.9%	1.6	$(5D, 2.5D)$

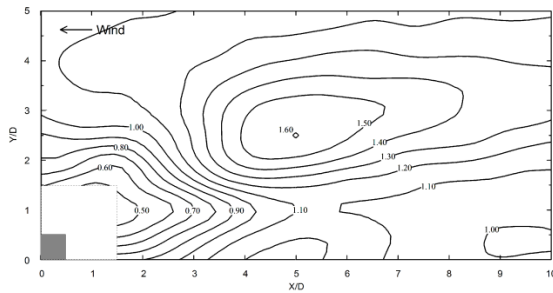


(a) Present study

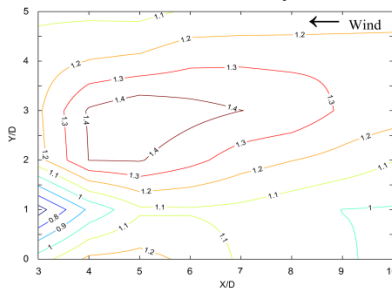


(b) Mara *et al.* (2014)

Fig. 7 IF contours of RMS along-wind moment



(a) Present study



(b) Mara *et al.* (2014)

Fig. 8 IF contours of RMS across-wind moment

The critical locations at which IF_{max} of the fluctuating across-wind load occurs reported by some previous studies are summarized in Table 1. The Reynolds number in these studies varies from 2.4×10^4 to 5.1×10^4 . It is noted that, in some studies, the peak interference factor IF_{max} or critical locations (X, Y) were presented in form of contour lines and the exact values were not explicitly given. In those cases, a range of IF_{max} and critical locations of are estimated from the contour lines. It can be observed from Table 1 that, although measurements were made on building models with various aspect ratios and at different turbulence intensities, the critical location of peak IF in the present study $(X/D = 5, Y/D = 2.5)$ agrees well with the previous results in which IF_{max} occurs in the range of $X/D = 4 \sim 6$ and $Y/D = 2.5 \sim 3$. For IF_{max} , Taniike (1992) reported a value of 2.5~2.6, which is significantly larger than the values in other studies and this might be caused by the low turbulence intensity used. The turbulence intensity in Mara *et al.* (2014) and the present study was 10.2% and 8.9%, respectively. In the tests of Sakamoto and Haniu (1988) and Khanduri *et al.* (2000), simulated atmospheric boundary layer flow was used as the approaching flow and some degree of turbulence was not stated. Under a relatively low level of turbulence in the incoming wind, the upstream building wake is well-correlated and this would enhance the wind load on the downstream building (Khanduri *et al.* 1998). With a higher turbulence intensity, the approaching turbulence tends to dampen the strength of the wake and leads to less prominent magnification of wind load and relatively lower IF (Khanduri *et al.* 1998, Kareem 1987, Mara *et al.* 2014). This also explains why the present value of IF_{max} is slightly larger than that of Mara *et al.* (2014).

For the tandem arrangement (i.e., $Y/D = 0$), the interfering building provides shielding for the principal building when they are closely spaced ($X/D = 1.5$ to 2.5). A region of $IF > 1$ is observed between $X/D = 3$ and 7 , and the largest value is $IF = 1.24$ at $X/D = 4.5$. The corresponding value in Mara *et al.* (2014) is $IF = 1.25$ at $X/D = 5$. Generally, there is a good consistency between the two studies. For the side-by-side arrangement, Taniike (1992) found that, with low approaching turbulence intensity, the magnification of RMS across-wind load by up to 50% occurred at $Y/D = 2$ to 4 . However, for the open exposure in present study, $IF < 1$ is observed at the locations $Y/D = 1.5$ to 3 where the interfering building can provide shielding for the principal building.

3.1.3 Torsion IF

The IF contours of RMS torsion are shown in Fig. 9. It can be found that IF is higher than unity in a large area ($X/D = 4$ to 10 , $Y/D = 1$ to 5) which is also reported in Mara *et al.* (2014). The crest of the region of $IF > 1$ roughly lies on the line of $Y/X = 1/4$ (e.g., $X = 2$, $Y = 0.5$ and $X = 6$, $Y = 1.5$). In these positions, the principal building is impinged by the shear layer of the upstream building leading to asymmetric fluctuations in the wind load of the principal building. In the tandem arrangement, the presence of interfering building decreases the fluctuating torsion of the principal building at $Y/D = 1.5$ to 5.5 . This may be due to the small pressure fluctuations on the walls of the principal building when being immersed in the wake of the interfering building. As the distance becomes larger ($X/D > 5.5$), the interfering building leads to an increase of fluctuating torsion. This may be due to the fact that the RMS torsion moment of an isolated symmetric building would be quite low; and the introduction of any turbulence in the approaching flow can result in a significant increase for RMS torsion. In the side-by-side arrangement, shielding for the principal building occurs when two buildings are close $Y/D < 2$ and, with increase of distance between two buildings, IF of the fluctuating torsion becomes higher than 1.

3.1.4 Pressure distribution

Besides the overall wind loads, local wind pressure distributions are also modified by presence of a surrounding building and this can have significant implications in the cladding design. The pressure distribution also helps in the understanding of interference mechanisms (e.g., Kim *et al.* 2013).

Fig. 10(a) shows the mean wind pressure coefficient on the windward surface of the principal building when the interfering building is located at ($X/D = 1.5$, $Y = 0$). It can be found that when two buildings are so closely located, wind pressures on the front surface become negative due to the principal building being immersed in the building wake. As wind pressures on the front surface and the back surface act in opposite directions, the disappearance or even the inverse of overall along-wind load observed around this location is reasonable. When compared with the result obtained in the wind tunnel test of Kim *et al.* (2013), at which $Re = 3.85 \times 10^4$, it can be seen there is generally a good consistency between the two studies except for regions near the edge of the surface. This is probably because the pressure taps near the edge in the present study are not arranged as close to the edge as those in Kim *et al.* (2013) which used a building model of a larger geometry-scale (1:400) and larger sizes.

The situation of two buildings positioned side-by-side is another typical arrangement which can lead to large interference (Yu *et al.* 2015). Part (i) of Fig. 10(b) shows IF contour of the mean wind pressure coefficient on the side surface of the principal building facing the interfering building located at $Y/D = 1.5$. It can be observed that wind pressure near the leading edge (right-hand side in the figure) is largely magnified by the channeling effect. Part (ii) of Fig. 10(b) shows the result reported in Yu *et al.*

(2015), in which the length scale was 1:400, $Re = 7.7 \times 10^4$, and the interfering building was located at $Y/D = 1.8$. Very similar distribution pattern of wind pressure can be found in the two studies. The extreme values, both the largest and the lowest, of IF in this study have slightly higher magnitudes than those of the previous study. It is noted that the spacing between two buildings in this study is smaller than that of Yu *et al.* (2015) and, thus, this smaller channeling space can lead to more significant interference effects on the inner-side building surfaces.

3.1.5 Reynolds number and geometric scale effect

Building models tested in the present study have the geometric scale at 1:1000 and this is to facilitate the time resolved PIV measurements of wind flow fields in the next part of the study using the PIV system of limited capacity. This geometric scale is significantly smaller than those usually used in most previous studies (1:400 ~ 1:300). Although Reynolds number of the tests at $Re = 1.8 \times 10^4$, can satisfy the minimum requirement of $Re = 1.1 \times 10^4$ for sharp-edged structures (ASCE 2012), this value of Re is probably the lowest among all interference studies in the literature (Table 1). Furthermore, a minimum geometric scale of 1:800 is recommended in AWES (2001). Therefore, detail interference data of wind pressures, overall wind loads and critical locations leading to maximum magnification have been obtained in the preceding sections and compared with results of previous studies. The comparisons support that the present data obtained at a geometric scale 1:1000 and $Re = 1.8 \times 10^4$ are consistent with those in the literature obtained at larger geometric scales (1:300 ~ 1:400) and higher Reynolds numbers ($2.4 \times 10^4 \sim 7.7 \times 10^4$). This ensures that the underlying mechanism of interference phenomena observed in the present wind tunnel experiments is valid for prototype buildings.

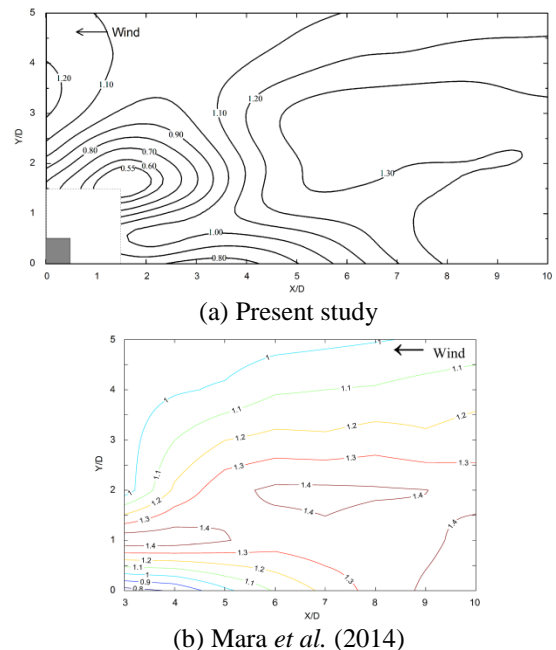
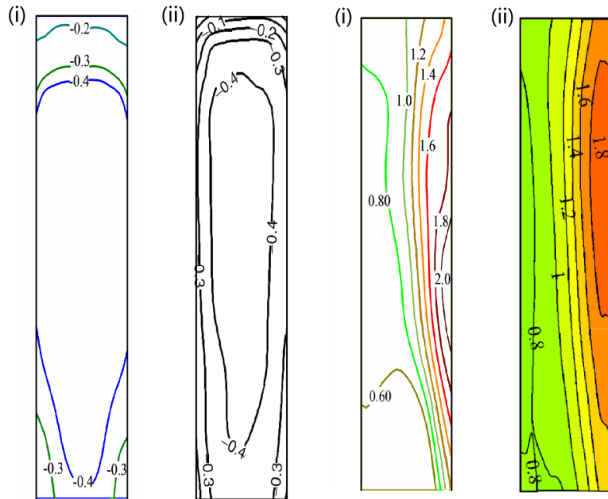


Fig. 9 IF contours of RMS torsion



(a) tandem arrangement ($X/D = 1.5$), C_p on windward face: (i) present study, (ii) Kim *et al.* (2013)
 (b) side-by-side arrangement, side face facing interfering building, IF on mean pressure: (i) present study ($X/D = 1.5$), (ii) Yu *et al.* (2015) ($Y/D = 1.8$)

Fig. 10 Surface pressure distribution on principal building

3.2 Synchronized measurement of wind pressure and flow field for tandem arrangement

A distinctive characteristic of the tandem arrangement is that the upstream building usually provides shielding for the along-wind load on the downstream building. For across-wind load, it is not always true. As shown in Section 3.1.2, a directly upstream building can either increase or decrease the fluctuating across-wind load depending on the distance between two buildings. In order to investigate the reason for this change from magnification to deduction of wind load, wind flow fields at two locations, $X/D = 2.5$ and $X/D = 5$, leading to increase and decrease of wind load, are studied with synchronized PIV and pressure measurements.

Fig. 11 shows the spectra of along- and across-wind moments for the isolated building case and the two interference cases of $(X/D, Y/D) = (2.5, 0)$ and $(5, 0)$. For the isolated single building, the across-wind moment spectrum shows a sharp spectral peak at Strouhal number $St \approx 0.10$. This is due to vortex excitation (e.g., Lam *et al.*, 2008). It can be seen that the across-wind fluctuating power spectral densities of the tandem case of $X = 5D$, of which IF of the across-wind moment equals 1.22, are higher than the isolated case for almost all frequencies and the spectral peak also has higher density. However for the case of $X = 2.5D$, of which IF of the across-wind moment is 0.95, there is an inconspicuous peak near Strouhal number $St = 0.07$ and for all frequencies the power is higher than the isolated case except around the spectral peak region.

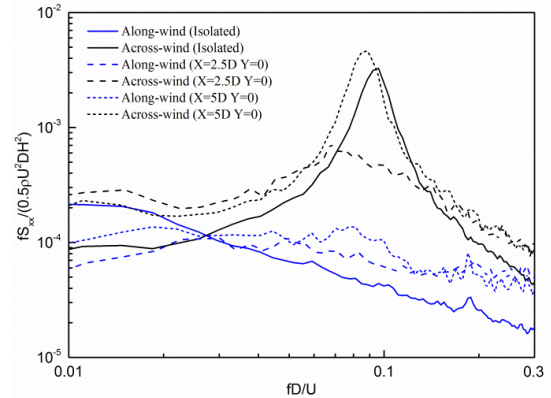


Fig. 11 Normalized spectra of along-wind and across-wind moments

3.2.1 Instantaneous and time-averaged wind flow field

PIV measurements are made to the flow field at a height of 170 mm above the floor, that is, $\sim 0.94H$. This is the height of the top level of pressure taps on the building surfaces. The time-averaged mean flow field for the tandem location of $(X = 2.5D, Y = 0)$ is presented in Fig. 12(a). The wind speeds are normalized by the reference wind speed at the building roof height. In order to capture the main flow characteristics between the twin buildings, the laser sheet is shone from the upper side of the figure. Thus, there is a region at the other side of the buildings, where the laser light is partly blocked by pressure tubes and building surfaces, and, therefore, wind field measurement in this region is likely to be inaccurate. The region is marked in the figure. It is obvious that the downstream building is enveloped by the wake of the upstream building and the flow pattern around the downstream building largely differs from that of the upstream building. Unlike the normal flow pattern around a square cylinder, there is almost no flow separation near the leading edge of the downstream building and wind just flows past the side surfaces of the building in almost parallel directions. Therefore, periodic vortex shedding usually observed from a single building can hardly occur for this arrangement and, thus, the across-wind fluctuating load due to vortex excitation is decreased to a large extent for this case. However, the overall IF of the RMS across-wind moment is 0.96 which indicate that the fluctuating wind load does not experience a large reduction.

The contours of along-wind and across-wind turbulence intensity are shown in Figs. 12(b) and 12(c). It is obvious that the turbulence intensity between the two buildings is around 0.2 - 0.3 and is much higher than turbulence intensity of the approaching flow, which is 0.087 at the roof height.

Therefore, the increased turbulence in the approaching flow due to the building wake is very likely to lead to an increase of overall fluctuating wind force, both in the along-wind and across-wind directions. This is confirmed by the across-wind spectrum in Fig. 11. It can be seen that the background fluctuating energy of across-wind moment at almost all frequencies is much larger than that of a single building except for the spectral peak region.

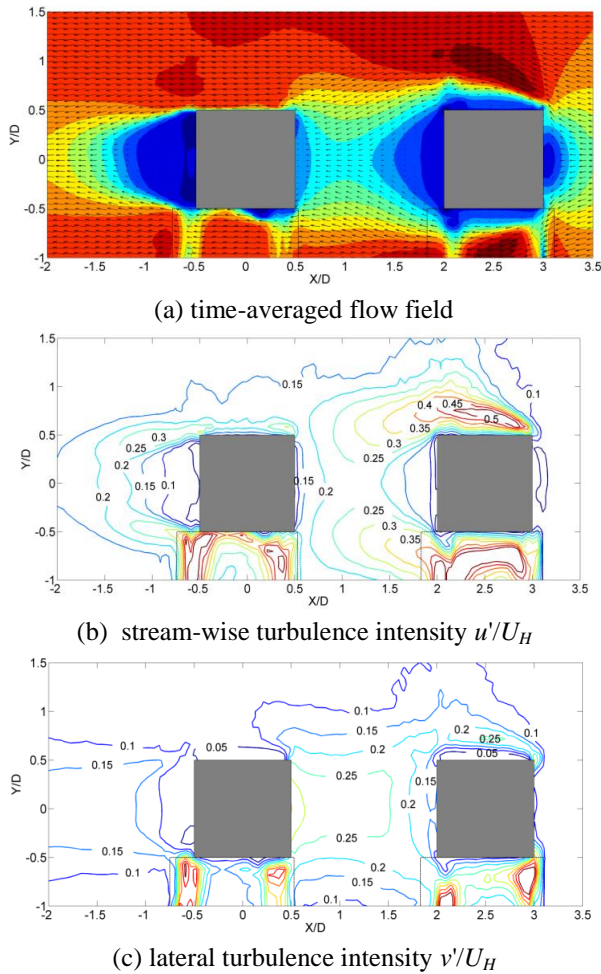


Fig. 12 Flow field of tandem configuration ($X = 2.5D$, $Y = 0$)

Fig. 13 shows the instantaneous flow field of the tandem configuration $X = 2.5D$ for a short sequence of time instants from 3.64 s to 3.69 s. It can be seen that, at all the time instants, the two shear layers from the upstream building reattach on the two side surfaces of the principal building. And just as illustrated by the mean flow field, wind just flows past the side surfaces smoothly and no separation flow can be observed.

Fig. 14(a) shows the time-averaged mean flow field for the tandem configuration $X = 5D$. Compared with the configuration $X = 2.5D$, the flow pattern around the downstream principal building is more similar to an isolated building. Due to the wider spacing between two buildings, wind flow in the gap region is able to redistribute itself so that the mean flow towards the windward face of the principal building follows the parallel direction rather than the slightly converging direction as in Fig. 12. Flow separation is now observed to occur at the leading building corners. For the across-wind spectrum (Fig. 11), except for the peak region, the background power spectral densities of this configuration are larger than that of a single building and slightly smaller than the configuration of $X = 2.5D$. The contours of turbulence intensity of the two velocity components are presented in Figs. 14(b) and 14(c). It can be

observed that, as the spacing between two buildings becomes larger in this configuration, the building wake recovers within the longer distance and the turbulence intensity between two buildings becomes smaller than the configuration of $X = 2.5D$ but is still higher than the ambient wind flow.

Although lower turbulence is found in the region between two building for the configuration $X = 5D$ than the configuration $X = 2.5D$, the fluctuating across-wind load is magnified by up to 22%. The moment spectra in Fig. 11 supported that the increase of fluctuating energies come from frequencies centered at the spectral peak. However, it is expected that periodic vortex shedding from the principal building is interrupted by the upstream building. There have been suggestions that, the fluctuating force acting on the principal building may result from the building wake of the upstream building (Bailey and Kwok 1985, Taniike 1992).

To find the periodic flow phenomenon which induces the periodic force, instantaneous flow fields from 1.20 s to 1.25 s are shown in Fig. 15(a) to 15(f). It can be found that as vortices tend to be shed from the upstream building, the streamlines swing sideways in a coherent manner and meander down to the downstream building; and this lateral oscillation of the building wake envelopes the downstream building. A relationship between the across-wind force on the downstream principal building and the sideways meandering of the upstream building wake may exist (Fig. 15(g)). When the across-wind force reaches the highest value in one period at 1.20 s, the oscillating wake of the upstream building swings to the lowest lateral extent and streamlines with downwards oblique direction are found incident on the downstream building, which may result in unbalanced flow separation at the two windward corners and eventually unequal suction pressures on the two side walls. As the wake moves up towards the upper surface, the across-wind force decreases gradually and, then, reaches the trough at 1.23 s. Afterwards, the wake moves back towards the lower surface (1.24 s) and the across-wind force changes direction, and reach a crest again at 1.25 s.

The connection between across-wind force and sideways oscillation of the upstream building wake is further studied with correlation analysis. Fig. 16 shows the cross correlation coefficient between the across-wind force on the principal building and the lateral velocity component $v(t)$ on the wake centerline but at different locations between the two buildings. The results show that the quasi-periodic across-wind force fluctuations on the downstream building are strongly correlated with the sideways meandering of the upstream building wake. Both oscillations are quasi-periodic to the vortex shedding frequency from the upstream building and the strongest correlation occurs for the velocity at $(x = 2D, y = 0)$ with a correlation coefficient of -0.36 .

3.2.2 Peak wind force events

An attempt to reveal the dominant large-scale coherent characteristics of the flow field during the occurrence of peak across-wind forces on the downstream building is made using the conditional sampling method (Lam and Zhao 2002).

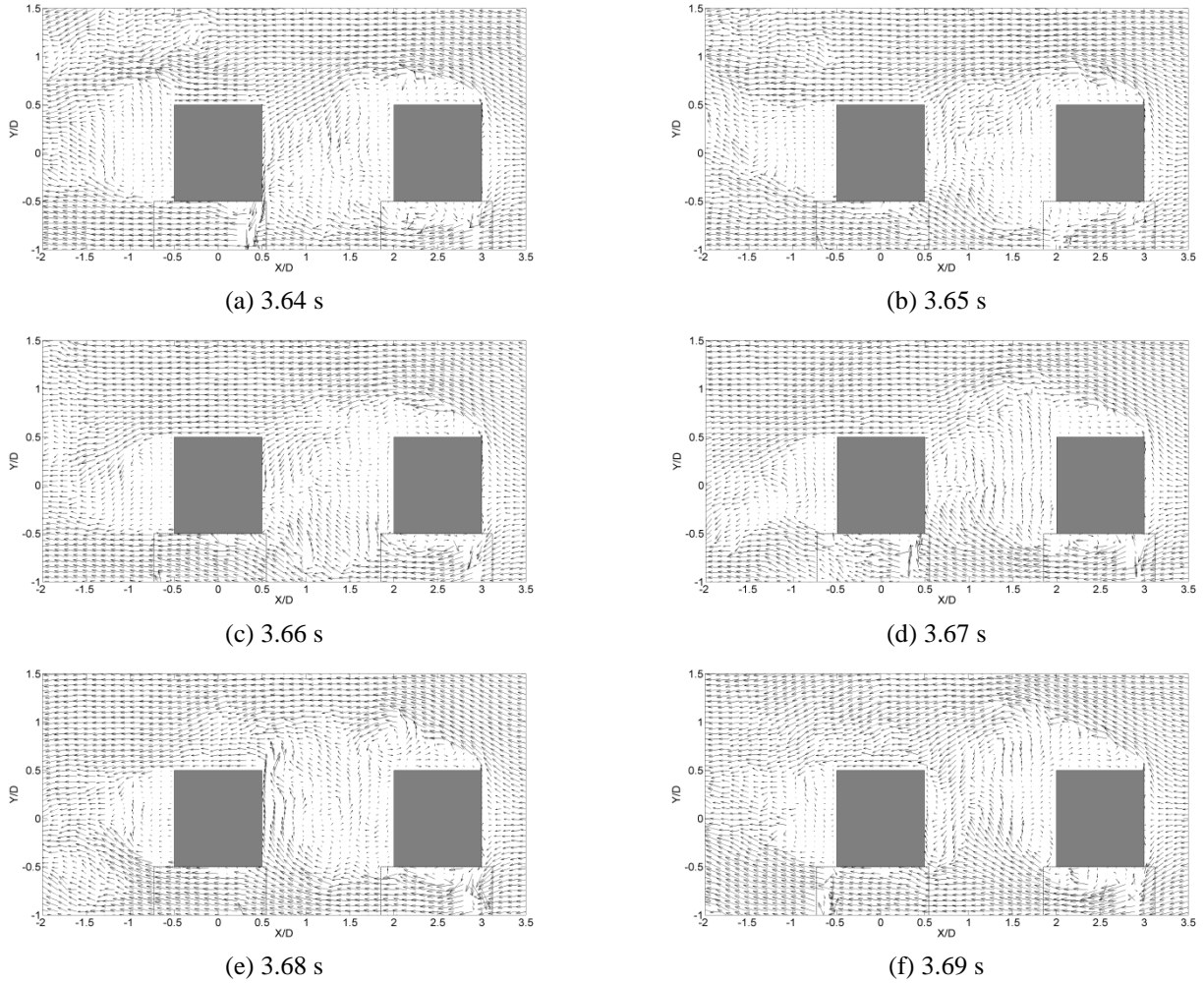


Fig. 13 Instantaneous flow field of tandem configuration ($X = 2.5D$, $Y = 0$)

A peak across-wind force event on level i was determined by a peak in the force time history with magnitude above a trigger level. The trigger level was set using a “peak factor” g and the root-mean-square value of across-wind force coefficient σ_{C_F}

$$\hat{C}_{F_{\text{across},i}} = g\sigma_{C_F} \quad (5)$$

With zero mean across-wind forces and by using $g > 0$ or $g < 0$, both the peak across-wind force events in either of the two sideways directions could be identified and used as triggers for the conditional sampling. The value of g affects the stringency of peak event selection. For a signal with a Gaussian distribution, a peak factor of magnitude between 2 and 3 has been shown to be appropriate (Lam and Zhao 2002). In this study, a less stringent value of $g > 2$ or $g < -2$ was chosen so as to increase the ensemble size of peak load events.

Figs. 17(a) and 17(b) show the conditionally sampled wind velocity fields and wind pressures on the horizontal plane at mid-height ($h/H = 0.5$) corresponding to the instants of peak maximum and minimum across-wind forces. This is for the tandem arrangement of $5D$ building

separation at which magnifications of across-wind load fluctuations occur. For comparison, conditionally sampled flow field of an isolated building are also obtained (Figs. 17(c) and 17(d)). It is obvious that the wake flow pattern of the downstream building at peak force events is totally different from that of the isolated building. For the isolated building, a fully developed vortex with a size close to the building width is clearly observed in the building near wake at the instant when the across-wind force reaches a peak in either direction.

Figs. 17(c) and 17(d) show that the full-sized vortices are centered at $x/D \approx -1.2$. Fluid circulation associated with the vortex induces fast moving flow to separate at one side face of the building and the induced high suction pressures on that side face result in the peak across-wind force acting in the direction away from that side wall. In other words, the quasi-periodic across-wind forces on the isolated building are attributed to the development and dynamics of vortices shed from the building.

When the building is downstream of an interfering building in the tandem arrangement, the development of full-sized vortices cannot be evidently observed in the downstream building wake.

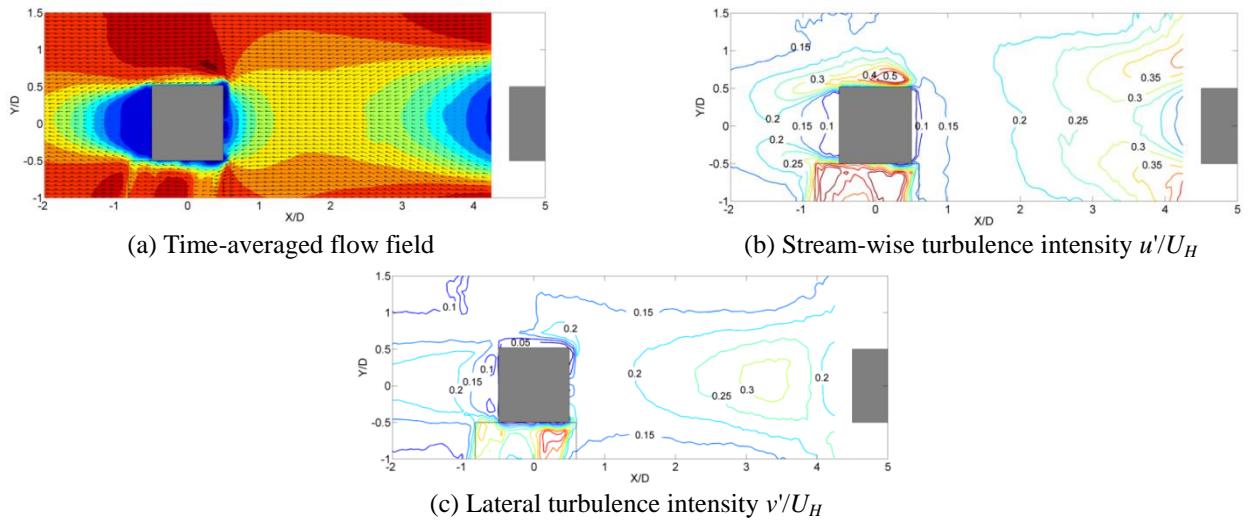


Fig. 14 Flow field of tandem configuration ($X = 5D, Y = 0$)

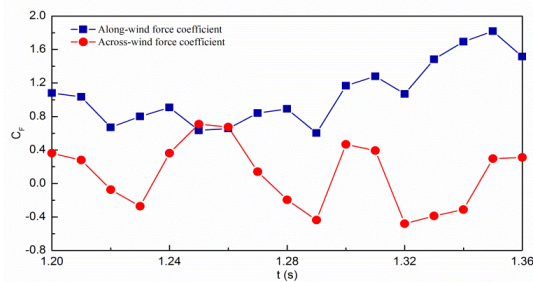
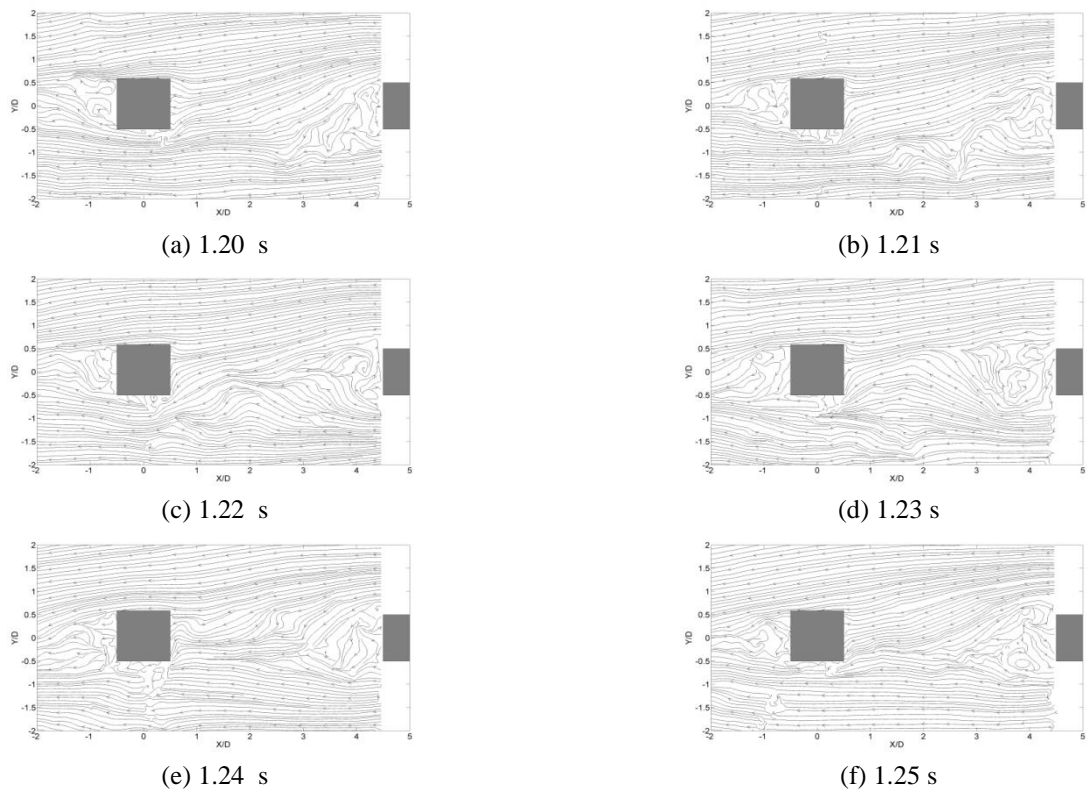


Fig. 15 Instantaneous flow field of tandem configuration ($X = 5D, Y = 0$)

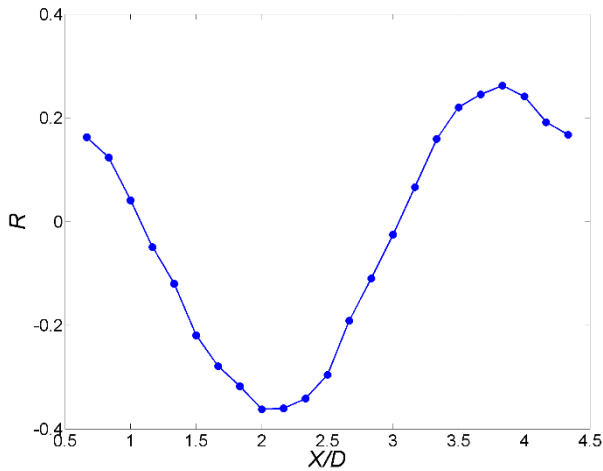


Fig. 16 Cross correlation between across-wind force and lateral velocity fluctuations at different location of wake, along $Y = 0$

Despite this impairment of coherent vortex shedding from the principal building, the fluctuating across-wind forces have larger magnitudes than the isolated building case (Fig. 11). The results of Figs. 17(a) and 17(b) suggest that this load magnification is caused by the large-scale meandering of the incident flow to the downstream building. The quasi-periodic flow-stream meandering in a near sinusoidal manner is intrinsic to the vortex shedding wake of the upstream building.

At the occurrence instants of a peak maximum (upwards acting) across-wind force event (Fig. 17(a)), the upstream building wake leads to a flow stream with upwards direction incident on the downstream building. This instantaneous oblique incidence on the building results in strong flow separation at the windward corner of upper side face, inducing strong suction pressure on that side wall. On the other hand, the veered wind flow passes the lower side wall smoothly, resulting in relatively smaller suction pressure comparing with that of the isolated building. This difference in suction pressures on the two side walls is responsible for the occurrence of the peak maximum across-wind forces (upwards acting) on the downstream building. A grossly reverse flow pattern is observed for the instant of peak minimum forces in Fig. 17(b). At this instant, the upstream building wake oscillates downwards near the windward wall of the downstream building and results in large suction pressure on the lower side wall.

A similar mechanism of incident wind flow directions can be observed on the instantaneous velocity fields in Fig. 15. However, the relationship is now as evidently revealed by the conditional sampling results.

3.2.3 Phase-averaged flow field

It is evident from the conditional sampling results that the flow around the downstream building is dominated by the oscillating wake of the upstream building, which being accompanied with incoherent turbulent fluctuations, generates amplified quasi-periodic across-wind loads on the downstream building. While the conditional sampling

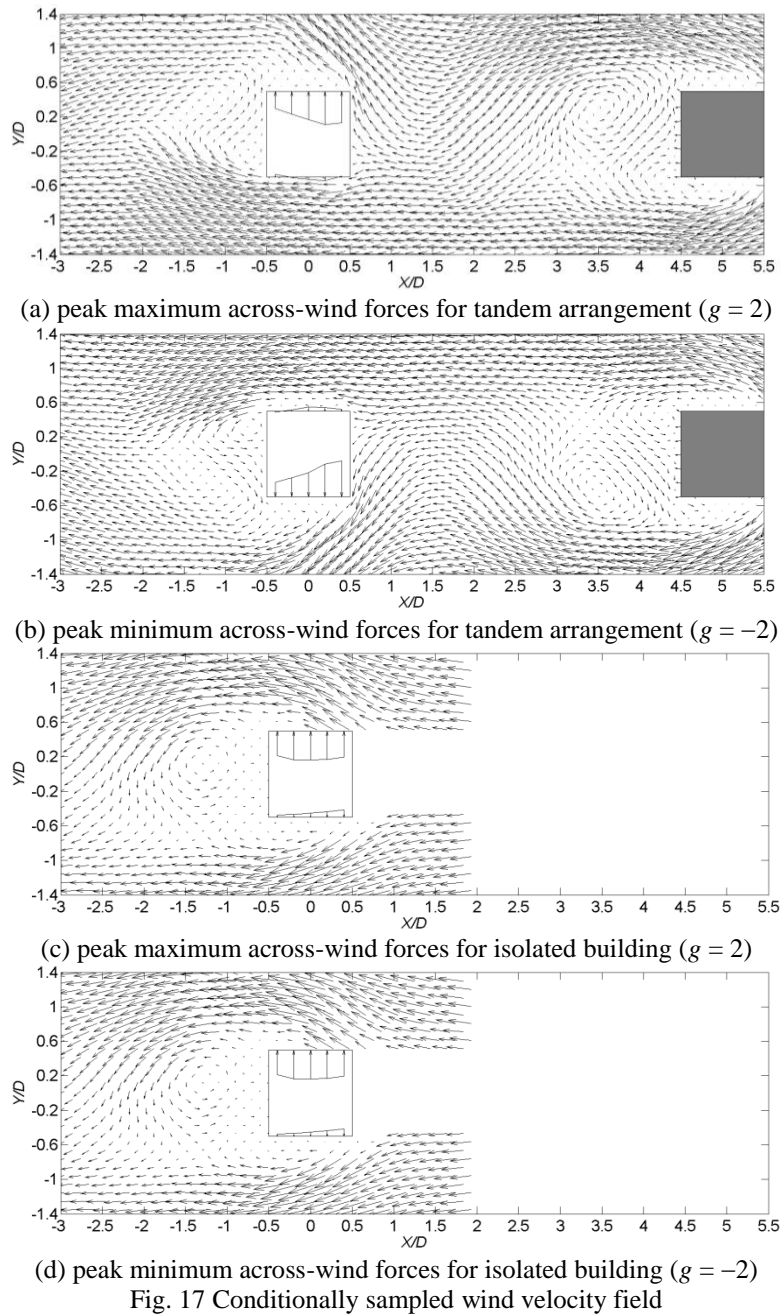
technique reveal the peak flow events, the typical features for the more commonly occurring quasi-periodic flow cycles can be explored with the aid of the Hilbert transformation technique (Wlezien and Way 1979). In the present quasi-periodic flow, the fluctuating across-wind force is a good signal to reveal the phase of the coherent flow patterns using Hilbert transform. The Hilbert transform $\hat{r}(t)$ allows the calculation of the instantaneous envelope and phase from a signal $r(t)$

$$\hat{r}(t) = \frac{1}{\pi} \int_{-\infty}^{\infty} \frac{r(\xi)}{\xi - t} d\xi \quad (6)$$

whereby a complex time signal is obtained as $z(t) = r(t) - i\hat{r}(t)$ which can be written in the form of $z(t) = A(t) e^{i\phi(t)}$, where $A(t)$ is the instantaneous envelope of $z(t)$, and $\phi(t)$ is the instantaneous phase.

The measurement data on the horizontal plane at mid-building height is chosen here to be studied. Similar to the whole building, the power spectrum of the across-wind force at this height also exhibits a peak at $St = nD/U_H \approx 0.09$ corresponding to a vortex shedding frequency at 16.0 Hz in model scale (Fig. 11). As the Hilbert transformation is sensitive to noise, the quality of the results is improved by applying a fifth-order digital Butterworth band-pass filter with a band-pass filter at 11–21 Hz to the across-wind force signal before applying the Hilbert transform. Then the phase angle was determined from the filtered signals for each instant of the flow fields. The flow fields were then classified according to this phase angle into windows of width $2\pi/8$ corresponding to 8 phase angles in a period.

An example of the filtered signal is shown in Fig. 18(a). Some irregularities in the signal periods and amplitudes can be observed when the quasi-periodic component of the across-wind flow is weak and overcast due to strong turbulent background flow fluctuations. These instants of flow irregularities need to be detected and removed so as to reveal the periodic flow signatures. This is achieved by applying a signal sorting step based on thresholds on both the period and amplitude. If a period is too far from the mean period or if the amplitude is too small, that period and half a period before and after are rejected as shown in Figs. 18(b) and 18(c). The sensitivity of threshold selection on the phase-averaged flow field is tested. Fig. 19 shows the phase-averaged u and v velocity components at different x/D locations (along $y/D = 0$) at the phase angle $\phi = 0$ for different values of the thresholds imposed on the period (between 10% and 60% deviated from the mean period by steps of 10%) and on the amplitude (from 0.1 to 0.4 by steps of 0.05). It can be seen that two groups of profiles are obtained. One group (severe value) is sorted by the most severe threshold values which result in inadequate instants to achieve converged statistics. The other group (moderate value) is sorted by values of thresholds between 30 and 50% for the period and 0.1 to 0.3 for the amplitude. Changing the threshold criteria within this range leads to relative small differences of profiles comparing with those values outside this range.



Thus, a threshold of 40% on the period and a threshold of 0.2 on the amplitude of normalized cross-wind force on mid-height is chosen. After this sort, about 86% of the signal is chosen for the calculation of the phase-averaged flow fields. Within the sampling time of measurement at 18.25 s, this is equivalent to about 228 quasi-periods of cross-wind excitation.

The phase-averaged flow patterns at $\pi/2$ phase intervals are shown in Fig. 20. The corresponding phase-averaged cross wind force coefficients for each phase are presented in Fig. 21. The development of vortex shedding and the consequent temporal cross-wind force acting on the building shows a good consistency with the instantaneous PIV results in Fig. 15 and the conditional sampling results in Fig. 17. The differences are that the phase-averaged

results are able to show more clearly the flow signatures of the large-scale building wake vortices than the instantaneous flow results which are masked by background turbulence and flow irregularities. On the other hand, during the occurrence instants of the infrequent very large cross-wind loads, the conditional sampling results reveal the role of much stronger vortices than the phase-averaged vortices in a typical quasi-periodic cycle of cross-wind excitation.

The phase-averaged results at phases $\varphi = 0$ to $3\pi/2$ in Fig. 20 clearly revealed the sideways meandering and oscillation of the upstream building wake and the consequent cross-wind forces. At phase $\varphi = 0$ (Fig. 20(a)), the flow pattern is quite similar with the conditionally sampled peak minimum event (Fig. 17(b)) and the cross-wind force reaches its peak minimum value. At this time,

the upstream building wake swings to form a region of crest-shaped streamlines immediately upwind of the downstream building and on the lower part of the wake. This makes the flow incident onto the windward wall of the downstream building, especially onto its lower part, with at a downward oblique direction and at fast speeds. Strong separation thus occurs at the lower building corner, as revealed by the peak vorticity contour lines there. Coupled with the relatively smooth flow on the upper side wall, a peak across-wind force is generated acting in the downward direction.

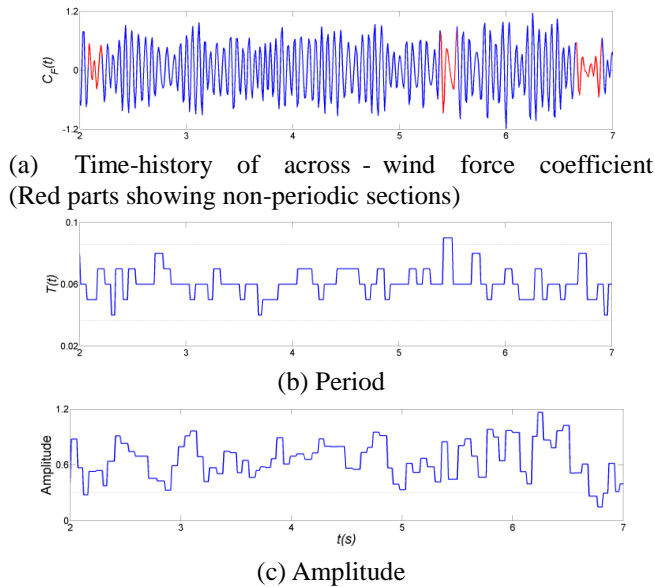


Fig. 18 Signal sorting based on period and amplitude

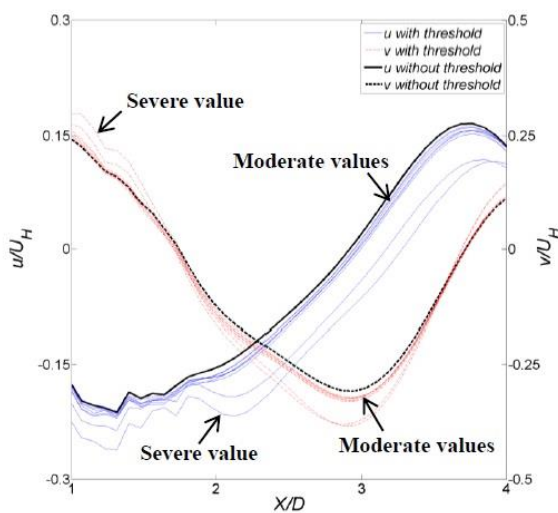


Fig. 19 Phase-averaged velocities for different values of threshold. See text for details

As the upstream building wake swings to phase $\varphi = \pi/2$ (Fig. 20(b)), there are no streamlines of crest- or valley-shape in proximity to the downstream building. Some flow separates at the upper side wall but with slow speeds. The flow along the lower side wall is faster but in a smooth direction along the wall. This explains the near-zero value of the across-wind force at this phase (Fig. 21).

At phase $\varphi = \pi$, the across-wind force reaches its maximum. The sideways oscillation of the upstream building wake now results in a region of valley-shaped streamlines immediately upwind of the upper part of the downstream building windward wall. This generates the same flow mechanisms as discussed previously in connection with Fig. 17(a) which produce large suction pressures on the upper side wall and the consequent peak across-wind force. The quasi-periodic flow cycle completes with the pattern at phase $\varphi = 3\pi/2$, which is almost the mirror image with respect to the wake centerline of that at phase $\varphi = \pi/2$.

4. Conclusions

Interference effects on aerodynamic wind loads between two identical tall buildings have been studied with wind tunnel tests on building models with a small geometry scale 1:1000. Independence of interference effect on Reynolds number is validated for this small scale from a comparison of the present results with previous studies using larger building models and at larger Reynolds numbers. The study then focuses on understanding in details the excitation mechanisms for interference effects of fluctuating wind loads on two tall buildings in tandem arrangement, especially on the fluctuating across-wind loads. Instantaneous velocity fields around the two buildings in tandem and their wind forces are measured simultaneously with synchronized PIV and pressure measurements. Conditional sampling technique and Hilbert-transform based phase averaging technique are applied to unveil the peak and quasi-periodic flow events responsible for the mechanism of interference between two buildings in tandem. The results obtained are summarized as follows.

- (i) Results of interference effect on aerodynamic wind loads between twin tall buildings, including overall wind forces, local pressure distributions and critical locations of maximum magnification of overall fluctuating wind load, of the present study are found to agree well with data of past wind tunnel experiments in the literature. This supports that the present tests carried out on building models of geometry scale 1:1000 and $Re = 1.8 \times 10^4$ could simulate interference behavior of prototype tall buildings as well as wind tunnel experiments using a larger geometry scale (1:300 ~ 1:400) and higher Reynolds numbers.

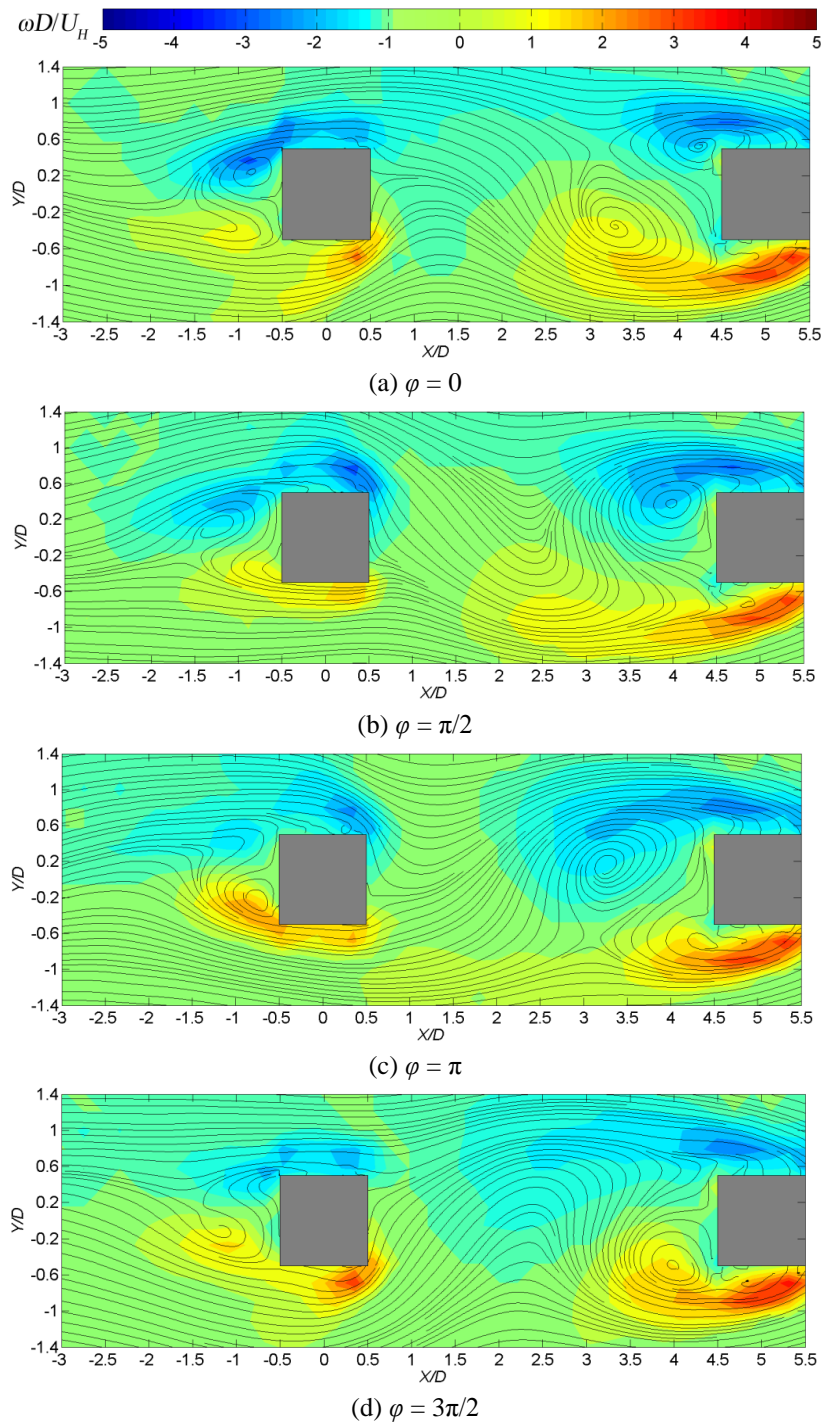


Fig. 20 Phase-averaged and resolved flow fields in one quasi-periodic cycle of across-wind force fluctuations. Flow streamlines and contours of normalized vorticity.

(ii) The fluctuating across-wind load is reduced when the upstream building is located in tandem at $X/D < 3$ while it is magnified as the distance between two buildings becomes larger than $3D$. When the two buildings are closely spaced, e.g., $X/D = 2.5$, the two shear layers separated from the upstream building reattach on to the two side surfaces of the downstream building. There is no flow separation around the leading edge of the downstream

building and, thus, regularly periodic vortex shedding, which is supposed to be the main source of across-wind fluctuation, is largely disrupted. When the distance between two buildings becomes larger, such as $X/D = 5$, coherent sideway oscillations of the wake from the upstream building govern the flow inside the building gap. The across-wind load on the downstream building also fluctuates periodically and strong correlation

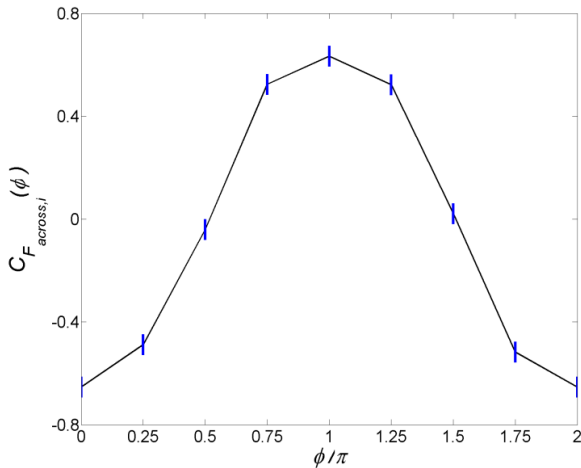


Fig. 21 Phase-averaged across-wind force coefficient on principal building ($X = 5D$, $Y = 0$)

between this across-wind load and the oscillation of the wake is found. By the conditional sampling and phase-averaged techniques, the coherent flow structures in the building gap are observed and the distinct relationship between the wake oscillation of the upstream building and the across-wind force on the downstream building is detected. The sideway meandering of the upstream building wake leads to streamlines incident on one side of the downstream building windward wall with significantly large oblique directions, leading to strong flow separation only at one corner of the wall. This produces large across-wind forces with quasi-periodicity in synchronization with the sideway oscillations of the upstream building wake.

Acknowledgements

The study is supported by a research grant awarded by the Research Grants Council of Hong Kong (HKU 713813E).

References

- ASCE (2012), "Wind tunnel testing for buildings and other structures", ASCE/SEI Standard. ASCE, New York, USA (49-12).
- Australasian Wind Engineering Society (AWES) (2001), "Wind engineering studies of buildings, Quality Assurance Manual", AWES-QAM-1-2001.
- Bailey, P.A. and Kwok, K.C.S. (1985), "Interference excitation of twin tall buildings", *J. Wind Eng. Ind. Aerod.*, **21**(3), 323-338.
- Cheng, L. and Lam, K.M. (2015), "Simultaneous measurement of wind velocity field and wind forces on a rectangular building", *Proceedings of the 14th International Conference on Wind Engineering*, Porto Alegre, June 2015.
- English, E.C. (1993), "Shielding factors for paired rectangular prisms: an analysis of along-wind mean response data from several sources", *Proceedings of 7th US National Conference on Wind Engineering*, Los Angeles.
- Gowda, B.H.L. and Sitheeq, M.M. (1993), "Interference effects on the wind pressure distribution on prismatic bodies in tandem arrangement", *Indian J. Technol.*, **31**, 485-495.
- Hui, Y., Tamura, Y. and Yoshida, A. (2012), "Mutual interference effects between two high-rise building models with different shapes on local peak pressure coefficients", *J. Wind Eng. Ind. Aerod.*, **104-106**, 98-108.
- Hui, Y., Tamura, Y., Yoshida, A. and Kikuchi, H. (2013a), "Pressure and flow field investigation of interference effects on external pressures between high-rise buildings", *J. Wind Eng. Ind. Aerod.*, **115**, 150-161.
- Hui, Y., Yoshida, A. and Tamura, Y. (2013b), "Interference effects between two rectangular-section high-rise buildings on local peak pressure coefficients", *J. Fluid. Struct.*, **37**, 120-133.
- Kareem, A. (1987), "The effect of aerodynamic interference on the dynamic-response of prismatic structures", *J. Wind Eng. Ind. Aerod.*, **25**, 365-372.
- Khanduri, A.C., Stathopoulos, T. and Bedard, C. (1998), "Wind-induced interference effects on buildings - a review of the state-of-the-art", *Eng. Struct.*, **20**(7), 617-630.
- Khanduri, A.C., Stathopoulos, T. and Bedard, C. (2000), "Generalization of wind-induced interference effects for two buildings", *Wind Struct.*, **3**(4), 255-266.
- Kim, W., Tamura, Y. and Yoshida, A. (2011), "Interference effects on local peak pressures between two buildings", *J. Wind Eng. Ind. Aerod.*, **99**(5), 584-600.
- Kim, W., Tamura, Y. and Yoshida, A. (2013), "Simultaneous measurement of wind pressures and flow patterns for buildings with interference effect", *Adv. Struct. Eng.*, **16**, 287-305.
- Kim, W., Tamura, Y. and Yoshida, A. (2015), "Interference effects on aerodynamic wind forces between two buildings", *J. Wind Eng. Ind. Aerod.*, **147**, 186-201.
- Lam, K.M. and Zhao, J.G. (2002), "Occurrence of peak lifting actions on a large horizontal cantilevered roof", *J. Wind Eng. Ind. Aerod.*, **90**, 897-940.
- Lam, K.M., Leung, M.Y.H. and Zhao, J.G. (2008), "Interference effects on wind loading of a row of closely spaced tall buildings", *J. Wind Eng. Ind. Aerod.*, **96**, 562-583.
- Larose, G.L. and D'Auteuil, A. (2006), "On the Reynolds number sensitivity of the aerodynamics of bluff bodies with sharp edges", *J. Wind Eng. Ind. Aerod.*, **94**, 365-376.
- Mara, T.G., Terry, B.K., Ho, T.C.E. and Isyumov, N. (2014), "Aerodynamic and peak response interference factors for an upstream square building of identical height", *J. Wind Eng. Ind. Aerod.*, **133**, 200-210.
- Sakamoto, H. and Haniu, H. (1988), "Aerodynamic forces acting on two square prisms placed vertically in a turbulent boundary-layer", *J. Wind Eng. Ind. Aerod.*, **31**, 41-66.
- Sakamoto, H., Haniu, H. and Obata, Y. (1987), "Fluctuating forces acting on two square prisms in a tandem arrangement", *J. Wind Eng. Ind. Aerod.*, **26**, 85-103.
- Saunders, J.W. and Melbourne, W.H. (1980), "Buffeting effects of twin upstream buildings", *Proceedings of the 5th International Conference on Wind Engineering*, Fort Collins.
- Taniike, Y. (1992), "Interference mechanism for enhanced wind forces on neighboring tall buildings", *J. Wind Eng. Ind. Aerod.*, **42**, 1073-1083.
- Taniike, Y. and Inaoka, H. (1988), "Aeroelastic behavior of tall buildings in wakes", *J. Wind Eng. Ind. Aerod.*, **28**, 317-327.
- Theunissen, R., Scarano, F. and Riethmuller, M.L. (2010), "Spatially adaptive PIV interrogation based on data ensemble", *Exp. Fluids*, **48**(5), 875-887.
- Willert, C.E., Gharib, M. (1991), "Digital particle image velocimetry", *Exp. Fluids*, **10**(4), 181-193.
- Wleziën, R.W. and Way, J.L. (1979), "Techniques for the experimental investigation of the near wake of a circular

- cylinder”, *Aiaa J.*, **17**(6), 563-570.
- Xie, Z.N. and Gu, M. (2004), “Mean interference effects among tall buildings”, *Eng Struct.*, **26**(9), 1173-1183.
- Xie, Z.N. and Gu, M. (2007), “Simplified formulas for evaluation of wind-induced interference effects among three tall buildings”, *J. Wind Eng. Ind. Aerod.*, **95**, 31-52.
- Yu, X.F., Xie, Z.N., Zhu, J.B. and Gu, M. (2015), “Interference effects on wind pressure distribution between two high-rise buildings”, *J. Wind Eng. Ind. Aerod.*, **142**, 188-197.
- Yu, X.F., Xie, Z.N., Wang, X. and Cai, B. (2016) , “Interference effects between two high-rise buildings on wind-induced torsion”, *J. Wind Eng. Ind. Aerod.*, **159**, 123-133.

CC